ENHANCEMENTS TO THE WATER EROSION PREDICTION PROJECT (WEPP) FOR MODELING LARGE SNOW-DOMINATED MOUNTAINOUS FOREST WATERSHEDS

Anurag Srivastava, Ph.D.,[1], Joan Q. Wu, Ph.D., P.E.,[2] William J. Elliot, Ph.D., P.E.,[3] Erin S. Brooks, Ph.D., P.E.,[4]

[1]Department of Biological and Agricultural Engineering, University of Idaho, Moscow, ID 83844; email: srivanu@uidaho.edu (Corresponding Author)
[2]Department of Biological Systems Engineering, Puyallup Research and Extension Center, Washington State University, Puyallup, WA 98371; email: jwu@wsu.edu
[3]US Depart of Agriculture, Forest Service, Rocky Mountain Research Station, Moscow, ID 83843; email: welliot@fs.fed.us
[4]Department of Biological and Agricultural Engineering, University of Idaho, Moscow, ID 83844; email: ebrooks@uidaho.edu

Presented at the 2015 EWRI Watershed Management Conference

Reston, VA, August 4-7, 2015

ABSTRACT

The Water Erosion Prediction Project (WEPP) model, originally developed for hillslope and small watershed applications, simulates complex interactive processes influencing erosion. Recent incorporations to the model have improved the subsurface hydrology components for forest applications. Incorporation of channel routing has made the WEPP model well suited for large watersheds. However, the model is still limited in modeling forested watersheds where groundwater baseflow is substantial, and where snow accumulation and melt dominate winter hydrology.

A linear-reservoir model was used to estimate baseflow and a double-threshold temperature approach was used to partition precipitation into snow and rain. A mountainous subwatershed of the Upper Cedar River watershed was chosen for WEPP application and assessment. Simulations were conducted for 1996–2011 to assess the model. The WEPP model reproduced the majority of observed streamflow peaks and the general trend of the hydrograph demonstrating its applicability to a large watershed where groundwater baseflow was significant.

1. INTRODUCTION

Snow-dominated mountainous watersheds are the principal source of freshwater in rivers and lakes (Christensen et al., 2008). Unlike small watersheds, large watersheds are often highly heterogeneous in climatic and physiographic settings (Singh, 1997). The interactions of climate with varying soil, vegetation, and geology in complex snow-dominated mountainous watersheds have a substantial effect on streamflow generation (Kuraś et al, 2008; Safeeq et al., 2013). The understanding and assessment of hydrology of such snow-dominated watersheds are important for sound management of aquatic ecosystems and water supply and demands.

Streamflow hydrographs can be separated into three major components: surface runoff, subsurface flow, and groundwater baseflow. Surface runoff typically contributes to peak discharges in a hydrograph. Subsurface lateral flow dominates the falling limb of a hydrograph and occurs when water flows laterally through soils.

Baseflow is generated from water stored in shallow aquifers (often unconfined) during dry seasons, represented by the recession part of the hydrograph. As the size of the watershed increases, baseflow plays an increasingly important role in the surface- groundwater interaction and in regulating streamflows, particularly during low-flow periods (Tague and Grant, 2009; Winter et al., 1998). The quantification of baseflow in areas where it substantially contributes to streamflow is crucial for monitoring and management of water resources.

Numerous studies have been focused on assessing the behavior of baseflow contribution to streams or rivers (Nathan and McMahon, 1990; Moore, 1997; Wittenberg, 1999). Observed recession curves from some of the recent investigations fitted the non-linear storage-outflow relationships (Moore, 1997; Wittenberg, 1999; 2003) possibly due to the presence of multi-reservoirs, flood-plain storage, variations in rainfall, evapotranspiration, thickness of the aquifer (Nathan and McMahon, 1990), and a decrease in saturated hydraulic conductivity of soil with depth (Wittenberg and Sivapalan, 1999). To simulate such complex surface-groundwater processes that contribute to non-linearity in baseflow, a sound understanding of a study area's geology is required, which is often lacking. Therefore, a linear-reservoir assumption is more commonly used in hydrological models for simulating groundwater baseflow (e.g., SWAT, Arnold et al., 1995; MIKE SHE, Storm and Punthakey, 1995; BROOKS 90, Federer, 2002).

Dooge (1960) developed a linear-reservoir model for estimating baseflow on the assumption that groundwater outflow is directly proportional to groundwater storage. Past studies supported the linear-reservoir model as a good approximation for baseflow recession (Zecharias and Brutsaert, 1988; Vogel and Kroll, 1992; Hornberger et al., 1998; Chapman, 1999). A number of studies also show the linear-reservoir approach to be adequate to represent baseflow recession (Fenicia et al., 2006; Brutsaert, 2008; van Dijk, 2010; Krakauer and Temimi, 2011).

Snow-dominated mountainous terrain exhibits high spatial and temporal variations in precipitation and temperature (Hamlet, 2011), which strongly influence the seasonal streamflow (Wu et al., 2012). Generally, precipitation increases and temperature decreases with elevation (Whitaker et al., 2003; Smith, 2007). Precipitations at low-, mid-, and high-elevations are, respectively, dominated by rain, a mix of rain or snow, and snow (Elsner et al., 2010).

Hydrologic models simulate snowpack accumulation dynamics by partitioning precipitation into rain and snow based on surface air temperature and either a single or a double-threshold partitioning methods (Maurer and Mass, 2006; Kienzle, 2008; Mizukami et al., 2013). For snow-dominated mountainous watersheds, a double-threshold partitioning approach is commonly adopted in hydrologic models to account for high spatial and temporal variability in precipitation and temperatures. The snow and rain phases of precipitation vary by storm and location that could result in variable threshold temperatures (Kienzle, 2008). Maurer and Mass (2006) and Dai (2008) reported that rain-snow partition temperatures vary considerably from location to location and storm to storm, and the threshold temperature may range from −2°C to 4°C. The United States Army Corps of Engineers (1956) based on field investigation in the Pacific Northwest region suggested a temperature range of −1°C

to 3°C for mixed snow and rain for hydrological modeling.

The Water Erosion Prediction Project (WEPP) is a physically-based, continuous-simulation, distributed-parameter model (Flanagan and Nearing, 1995). The model is based on the fundamentals of hydrology, hydraulics, plant science, and erosion mechanics (Nearing et al., 1989). The WEPP model was originally intended for crop- or rangeland and there are several applications on small or medium-scale watersheds where streamflow is mainly from surface runoff (Baffaut et al., 1997; Liu et al., 1997; Amore et al., 2004; Pandey et al., 2008; Abaci et al., 2009).

The addition of enhanced routines for subsurface lateral flow and deep percolation computations to WEPP enhances the model's applicability to small forest watersheds where subsurface lateral flow is a dominant process (Covert et al., 2003; Dun et al., 2009). However, WEPP applications to forest watersheds have resulted in underprediction of streamflow primarily due to the negligence of groundwater baseflow (Dun et al., 2009; Zhang et al., 2009). Brooks et al. (2011) showed good agreements between simulated and observed streamflow from large watersheds in the Lake Tahoe basin by bypassing stream channel algorithms and simulating streamflow from hillslope output from the WEPP model. Baseflow was simulated using a linear reservoir approach as a post-processing step from cumulative deep percolation losses from all hillslopes in the watershed. The most recent addition of channel routing algorithms to WEPP allows simulations of streamflow from watersheds with perennial flows (Wang et al., 2010). Incorporating a groundwater baseflow component in WEPP is necessary for applying WEPP to large watersheds where there is a significant contribution of groundwater baseflow to streamflow.

Presently, the WEPP model is limited to using a single-threshold temperature for rain and snow partitioning. Dun et al. (2010) and Hubbart et al. (2011) emphasized the limitations of using a single threshold in WEPP to distinguish precipitation phases and suggested the incorporation of a double-threshold rain-snow partitioning method to better represent snow accumulation processes.

The objectives of this study were (i) to develop and incorporate algorithms in WEPP (v2012.8) to estimate groundwater baseflow following the linear-reservoir approach; (ii) to enhance the WEPP winter routines by adopting a double-threshold approach for rain-snow partition, and (iii) to evaluate the performance of the modified WEPP model by applying it to a typical snow-dominated watershed in the US Pacific Northwest.

2. METHODS

2.1 WEPP Model

WEPP conceptualizes watersheds as a network of rectangular hillslopes and channels (Baffaut et al., 1997). Surface runoff and subsurface lateral flow from each individual hillslope is routed through the downstream channel network to the watershed outlet. A water balance output file is generated by the model that includes simulated daily surface runoff, deep percolation, evapotranspiration (*ET*), subsurface lateral flow, and total soil water for each hillslope and channel segment. Deep percolation in the current WEPP model (*v*2012.8) is the amount of the water that

drains vertically out of the soil profile or the model domain. The absence of a groundwater baseflow component in the current WEPP renders it difficult to assess water yield for large watersheds where a significant amount of baseflow contributes to streamflow.

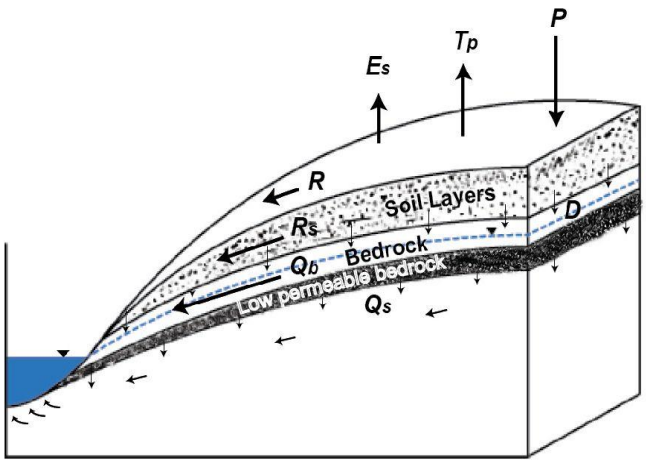

Fig. 1. Schematic of hillslope hydrologic processes. P, precipitation; E_s, soil evaporation; T_p, plant transpiration; R, surface runoff; R_s, subsurface lateral flow; D, deep percolation; Q_b, baseflow, and Q_s, deep seepage. The dotted blue line represents the groundwater level.

2.1.1 Incorporation of a Baseflow Component in WEPP

Fig. 1 shows the conceptualization of hillslope hydrologic processes, with a baseflow component added in WEPP. WEPP-computed daily deep percolation out of the soil profile is taken as recharge to the underlying aquifer, adding to the groundwater storage. Groundwater discharge to the adjacent stream contributing to the streamflow as baseflow is estimated following Dooge (1960). In addition, the groundwater may move further down into a deeper aquifer (Graham et al., 2010) and is considered lost from the model domain.

Equations 1 and 2 were used to compute baseflow and deep seepage. The storage-outflow relationship (Maillet, 1905) states that the outflow from the groundwater reservoir is a linear function of the storage.

The storage-outflow relationships for baseflow and deep seepage are

$$Q_b(t) = k_b \cdot S(t) \tag{1}$$

$$Q_s(t) = k_s \cdot S(t) \tag{2}$$

where Q_b is baseflow, Q_l is deep seepage, and S is the groundwater storage, all a function of time t [LT^{-1}], k_b and k_s are the baseflow and deep seepage coefficients, respectively, [T^{-1}]. Note that k_b represents the fraction of the groundwater storage at any given time that contributes to streamflow as baseflow, and ranges from 0 to 1. On the other hand, a positive value of k_s, ranging from 0 to 1, represents the fraction of the groundwater storage at a particular point in time that percolates from the upper aquifer to the lower aquifer, while a negative k_s value, ranging from $-\infty$ to 0, would represent the strength of the upward flow from the lower aquifer to the upper aquifer.

A global optimization algorithm, the Levenberg-Marquardt non-linear least-squares fit method (Vetterling et al., 1992) was implemented in WEPP to estimate the initial storage and the baseflow and deep seepage coefficients by minimizing the sum of squares of the difference between observed and simulated streamflow values.

2.1.2 Incorporation of Double Threshold Rain-Snow Partition in WEPP

In the WEPP *v*2012.8, snow accumulation, density, and melt are calculated on an hourly basis in the winter routine. The daily climate inputs of precipitation, temperature, and solar radiation are down-scaled to hourly values for snow accumulation and melt computations (Savabi et al., 1995). The density of freshly fallen snow is assumed to be 100 kg m^{-3}. Hourly fallen precipitation is determined as rain when the hourly air temperature is greater than the threshold temperature of 0°C and as snow otherwise. The depth and density of the snowpack are adjusted for new falling and drifting snow, snow settling, and snowmelt. Snowmelt occurs when the daily average temperature is greater than 0°C and snow density exceeds 350 kg m^{-3}.

To improve the WEPP simulation of snow accumulation as suggested by Hubbart et al. (2011) and Dun et al. (2010), we modified the rain-snow partition scheme to better simulate snow accumulation. We implemented the double-threshold rain-snow partition in the winter routine by adapting the approach of the US Army Corps of Engineers (1956). Hourly snowfall (P_{snow}), rainfall (P_{rain}), and mixed rain and snow (P_{mixed}) were determined based on snow density that is a function of hourly precipitation (P) and air temperature (T_a) as well as the upper (T_{rain}) and lower (T_{snow}) rain-snow partition thresholds:

$$\text{for} \quad T_a \geq T_{rain}, \qquad P_{snow} = 0, \quad P_{rain} = P;$$

$$T_a \leq T_{snow}, \qquad P_{snow} = P \cdot \frac{\rho_w}{\rho_s}, \quad P_{rain} = 0;$$

$$T_{snow} < T_a < T_{rain}, \qquad P_{mixed} = P \cdot \frac{\rho_w}{\rho}, \quad \rho = \rho_w - (\rho_w - \rho_s) \cdot \frac{(T_{rain} - T_a)}{(T_{rain} - T_{snow})} \qquad (11)$$

where ρ_w is the density of water (1000 kg m^{-3}), ρ_s is the density of fresh snow, and ρ is the density of mixed rain and snow assumed as a linear function of the air temperature when it is between the rain-snow thresholds.

2.2 Model Application

2.2.1 Watershed Description

Our model assessment focused on the Upper Cedar River watershed located in the Cascade Mountains of western Washington in King County, WA (Fig. 2). Known also as the Cedar River Municipal watershed, it is a protected, mountainous, forest watershed that supplies drinking water to the City of Seattle. The Cedar River generally flows northwest into the Cedar Lake (Wiley and Palmer, 2008). The 105-km^2 study watershed is upstream of Cedar Lake and ranges 477–1655 m in elevation (USDA NRCS, 2012). The watershed receives 70% winter

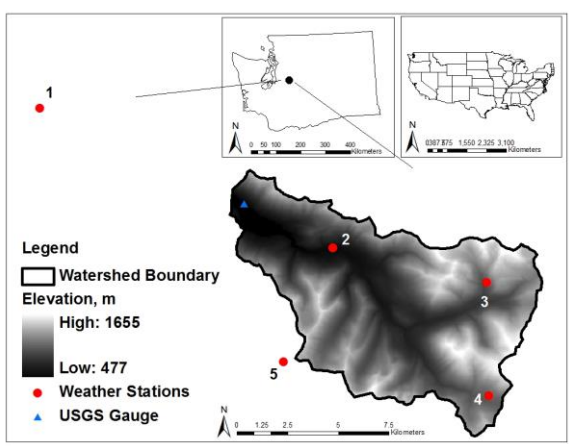

Fig. 2. Location of the study watershed. Dots denote SNOTEL and NCDC weather stations. The triangle represents the USGS stream gauging station.

precipitation (October–March) and 30% summer precipitation (April–September).

The two dominant soil series found on the uplands above the USGS stream gauge are Nimue (*andic haplocryods, loamy-skeletal, mixed*), a loamy sand that covers 56% of the watershed, and Altapeek (*andic haplocryods, sandy-skeletal, mixed*), a gravelly sandy loam that covers 15% of the watershed. Kaleetan (*typic haplohumods, loamy-skeletal, mixed, frigid*), a sandy loam, is typically found on the lowlands, covers 29% of the watershed (USDA, 2012). Along the soil profile, soil texture typically varies from sandy loam at shallow depths to extremely gravelly sandy loam near the 1520-mm depth (USDA, 2012).

The watershed is vegetated by a combination of old-growth and second-growth conifer forest. The old-growth forest is 250–680 years old and is mostly found on high elevations (Seattle Public Utilities, 2015). The second-growth forests at low elevations are younger than those at higher elevations due to harvest in the 20th century. Vegetation cover in the watershed generally falls into three forest vegetation zones. Franklin and Dyrness (1988) and Henderson et al. (1992) classified different vegetation zones by elevation and climate for western Washington and northwestern Oregon.

The underlying hydrogeology in the study area consists of a minor basaltic aquifer that is underlain by low-permeability intrusive igneous and metamorphic rocks on the uplands (USGS National Atlas of United States, 2013) and the unconsolidated-deposit (volcaniclastic deposits, andesite flows, and quaternary alluvium) aquifer in the lowland stream valley (Shellberg et al., 2010). The minor basaltic aquifer is adequately permeable for water to move laterally to recharge the unconsolidated-deposit aquifer that discharges water to nearby streams or lakes (USGS National Atlas of United States, 2013).

2.2.2 Climate and Streamflow Data

There are five weather stations and one USGS gauging station within and near the study watershed (Fig. 2, Table 1). The NOAA's National Climatic Data Center (NCDC) weather station is located downstream of Cedar Lake, and the other four NRCS SNOw TELemetry (SNOTEL) weather stations are located at higher elevations of the watershed. The NCDC has been recording weather data since 1940 while the four SNOTEL stations have weather data available from 1996 onwards. Weather data recorded at these stations include daily precipitation, maximum and minimum temperatures, and snow depth or snow water equivalent (SWE). The USGS gauging station is immediately upstream of Cedar Lake and has been recording daily streamflow since 1945.

Table 1. Elevation, average annual precipitation, maximum and minimum temperature, and percent precipitation as snow.

No.	Weather Stations	Source	Elevation (m)	Avg. Ann. Precipitation (mm)	Avg. Ann. Maximum Temperature (°C)	Avg. Ann. Minimum Temperature (°C)	Precipitation as snow (%)
1	Cedar Lake	NOAA-NCDC	475	2546	12.4	4.1	10
2	Mount Gardener	SNOTEL	890	2659	10.8	3.1	23
3	Tinkham Creek	SNOTEL	911	2683	10.8	1.7	32
4	Meadows Pass	SNOTEL	984	2427	10.8	1.4	40

5	Rex River	SNOTEL	1161	2704	9.4	2.0	43
Average				2606	10.4	2.3	34

Table 1 shows average annual precipitation, maximum and minimum temperatures, and elevation at each weather station in the watershed. Generally, precipitation increases with elevation (at about 0.13 mm m^{-1}) in winter, and decreases (at 0.01 mm m^{-1}) with elevation in summer. Mean air temperature decreases with elevation by 0.004 °C m^{-1} during both winter and summer months.

Snowfall in the region is highly dependent on elevation, typically starting at mid-November, peaking around mid-April, and melting by the end of May or June. Comparison of measured snow at the five weather stations indicates an increase in snowfall with elevation. On average, 34% of precipitation in the region falls as snow with the lowest amount of snow being observed at the Cedar Lake and the highest at Rex River.

2.2.3 WEPP Model Setup and Inputs

WEPP requires four main input files for both hillslope and channel elements: topography, climate, management, and soil. For WEPP simulations, we delineated the study watershed into hillslopes and channels using GeoWEPP, a geospatial interface of WEPP (Renschler, 2003), from a 30-m digital elevation model (DEM) (USDA NRCS, 2012). GeoWEPP uses TOPAZ (Topographic Parameterization, Garbrecht and Martz, 2000) to generate drainage networks for the watershed and topographic variables, such as slope length and width, slope gradient, and aspect for hillslopes and channels, from a DEM (Garbrecht and Martz, 2000). The minimum-source channel length and critical source area were set to 500 m and 25 ha, respectively, in delineating the drainage network to match the National Hydrography Dataset streams (USDA NRCS, 2012). In all, the TOPAZ-discretized watershed consisted of 253 hillslopes and 103 channels, including 52 first-, 21 second-, 7 third-, and 23 fourth-order channels.

Soil and vegetative characteristics of each hillslope or channel element were assigned from the STATSGO soil map (USDA NRCS, 2012) and the USFS vegetation map (Rolf Gersonde, Seattle Public Utilities, personal communication, 2014) with GeoWEPP using ESRI ArcGIS 10.1 software. Soil textural and hydraulic properties were extracted from the STATSGO database (USDA NRCS, 2012; Table 2). Soil albedo and erodibility parameters (rill erodibility, interrill erodibility, and critical shear) were obtained from the WEPP forest database (Table 3). The soil anisotropy ratio, which represents the dominance of lateral over vertical hydraulic conductivity of soil, was initially set to the default value of 25 for steep forest slopes, and was further calibrated for the study watershed. For this study, a single anisotropy ratio was used for the entire watershed.

Climate data recorded at the NCDC and SNOTEL stations in the watershed, such as daily precipitation and maximum and minimum temperatures, are available from the NCDC and NRCS websites. WEPP requires additional climate inputs, which include precipitation characteristics (event total and duration, normalized intensity, and time to peak intensity), solar radiation, dew-point temperature, wind speed, and

wind direction. These inputs were stochastically generated using CLIGEN *v*5.3 (Nicks et al., 1995), an auxiliary program included in the WEPP program package, based on the monthly statistics of the long-term historical weather data from the NCDC weather station near Cedar Lake.

Climate data recorded at the five weather stations (Table 1) were spatially interpolated using the Thiessen polygon method. Unique weather input files were developed and assigned to each hillslope within the five climate zones generated by the Thiessen polygon method. For channels, the lowest-elevation climate data from the Cedar Lake station were used as only one set of climate inputs is allowed for channels in the current version of WEPP.

Table 2. Soil characteristics in the study watershed.

Soil Series	Soil type	Sand (%)	Clay (%)	Organic Matter (%)	CEC (meq $100g^{-1}$)	Rock (%)	Hydraulic Conductivity (mm hr^{-1})
Nimue	Loamy sand	79.2	5.0	12.5	25.0	40	330
Kaleetan	Sandy loam	66.6	10.0	7.0	20.0	35	102
Altapeak	Gravelly sandy loam	66.6	10.0	7.5	7.5	30	102

Table 3. Major soil and management inputs.

Parameters	**Values**
Albedo	0.23
Initial saturation level (%)	80
Rill erodibility (s m^{-1})	5.0×10^{-4}
Interrill erodibility (kg s m^{-4})	4.0×10^{5}
Critical shear (Pa)	1.5
Anisotropy ratio	(25) 20*
Saturated hydraulic conductivity of restrictive layer (mm hr^{-1})	(0.41) 0.20*
Leaf Area Index	7[a], 10[b], 9[c]
Mid-season crop coefficient	(0.95) 0.75*
Readily available water	0.75
Initial groundcover (%)	100
Initial canopy cover (%)	0.79[a], 0.63[b], 0.58[c]
Day of senescence	250
Canopy height (m)	69[a], 61[b], 46[c]
Maximum root depth (m)	2

Values in parentheses are from the literature. Values with an asterisk are calibrated.
[a] Western hemlock; [b] Pacific Silver Fir; [c] Mountain Hemlock

The saturated hydraulic conductivity of the restrictive layer (K_{sat}) for basaltic-

andesite volcanic bedrock was reported by Belcher et al. (2002) as ranging 0.0017–250 mm hr^{-1} with a geometric and arithmetic mean of 2.5 mm hr^{-1} and 62.5 mm hr^{-1} for volcaniclastic sedimentary rocks and younger volcanic rocks, respectively. Todd and Mays (2005) reported a value of 0.42 mm hr^{-1} for basalt rocks. We set the K_{sat} value to 0.4 mm hr^{-1} initially (Table 3) and calibrated the value subsequently.

The management inputs for hillslopes were based on the default values for perennial forest in the WEPP database (Table 3). The maximum canopy height was taken from Dale et al. (1986). The percentage canopy cover and the leaf area index (*LAI*) were computed in ESRI ArcGIS 10.1 from available raster data provided by Seattle Public Utilities (Rolf Gersonde, personal communication, 2014). For channels, fallow management conditions in the WEPP database were used. The earth channel type was selected for the first- and second-order upland streams, and the channel-with-gravel-base type was chosen for the third- and the fourth-order lowland streams.

The WEPP *v*2012.8 has three channel-routing methods: linear kinematic-wave, constant-parameter Muskingum-Cunge, and modified three-point variable parameter Muskingum-Cunge that are appropriate for large watersheds (Wang et al., 2010). For this study, we chose the linear kinematic-wave method, which is suitable for steep and long channels (Wang et al., 2010).

2.2.4 Model Calibration and Performance Evaluation

All WEPP simulations were performed at a daily time step in a continuous mode. Daily streamflow records were separated into two periods: the first (January, 1996–September, 2003) for model calibration and the second (October, 2003–September, 2011) for model performance assessment. Four sensitive parameters in WEPP were identified and each was manually adjusted through a series of WEPP runs in three steps based on two widely used model performance statistical indices, namely, the Nash Sutcliffe Efficiency (*NSE*, Nash and Sutcliffe, 1970) and the deviation of runoff volume (D_v, Gupta et al., 1999). These indices were evaluated for simulated and observed daily SWE and streamflow for both the calibration and performance assessment periods.

In the first step of the WEPP model calibration, T_{rain} and T_{snow} parameters were optimized using the observed SWE at the SNOTEL sites. A single set of threshold temperatures was used for the entire study watershed. The calibrated T_{rain} and T_{snow} were 1°C and −1°C, respectively. The density of new fallen snow was adjusted to 175 kg m^{-3}, which was the average of the field-observed snow density ranging 150–200 kg m^{-3} at moderate and high elevations of the Cascade Range (Scott Pattee, USDA NRCS, Mount Vernon, WA, personal communication, 2014).

In WEPP, actual *ET* is computed from the reference *ET* following the FAO Penman-Monteith method (Allen et al., 1998) based on vegetation growth and environmental conditions. The mid-season vegetation coefficient (K_{cb}) and the ratio of readily available water to total available water in the root zone (p) were adjusted for the forest vegetation at the study watershed. The default values of K_{cb} and p for conifers were 0.95 and 0.70 (Allen et al., 1998). Both were calibrated to 0.75. Conifers tend to close their stomata and conserve water when soil water is limited

(Allen et al., 1998) as is the case in summer in the study area. In addition, deep-rooted mature conifers can maximize the use of soil water (Allen et al., 1998; Zhang et al., 2009).

After the calibration of the rain-snow partition and *ET* parameters, we calibrated K_{sat} for basaltic-andesite volcanic bedrock and soil anisotropy ratio simultaneously. The anisotropy ratio was varied from 1 to 5 and then to 30 in increments of 5 while K_{sat} was varied from zero to 0.6 mm hr^{-1} in increments of 0.2 mm hr^{-1}. Simulations with different levels of the anisotropy ratio were run against all levels of K_{sat}. For each WEPP run, the three baseflow parameters, S, k_b, and k_l (Equations 1 and 2), were optimized using the observed and WEPP-simulated streamflow data for the period of 1996–2003. For our study, we chose the optimum soil anisotropy ratio and K_{sat} to be 20 and 0.2 mm hr^{-1}, respectively.

Following the WEPP calibration, we assessed the model performance using the same inputs for the second period (October, 2003–September, 2011) of the streamflow observation, and the same statistical criteria of *NSE* and D_v. In addition to WEPP's ability to reproduce the daily observed SWE and streamflow, we also examined the simulated long-term annual water balance for both the model calibration and performance assessment periods.

3. RESULTS AND DISCUSSIONS

3.1 Snow Water Equivalent

Daily comparison of WEPP-simulated and SNOTEL-observed SWE for 1996−2011 is shown in Fig. 3. For the periods of model calibration (1996−2003) and model performance assessment (2004−2011), WEPP over- and underpredicted SWE, respectively.

For the period of model calibration, *NSE* for SWE ranged from 0.60 to 0.91 for the four SNOTEL sites, averaging 0.8, and D_v ranged from −19% to 11%, averaging −11%, indicating overprediction. For the period of model performance assessment, *NSE* varied from 0.34 to 0.42, averaging 0.38, and D_v ranged from 43% to 62%, with an average of 52%, suggesting underprediction. Generally, with increasing elevation, the agreement between the simulated and observed SWE improved for the calibration period, and decreased for the model assessment period (Fig. 3).

The trend of simulated SWE generally matched that of observed, with the exception of the years 2006, 2007, and 2010 for which the average *NSE* were −0.42, −0.65 and −0.82, and D_v were 93%, 87% and 90%, respectively (Fig. 3). The large discrepancies in simulated and observed SWE for these three years were possibly due to the replacements of standard temperature sensors with the extended-range temperature sensors. The temperature sensors at the Rex River and Meadows Pass, and Tinkham Creek and Mount Gardener SNOTEL sites were replaced in July, 2003 and May, 2005, respectively. Temperature sensors were replaced by the NRCS at Pacific Northwest SNOTEL sites to capture the temperature readings to −40°C (Julander, 2011). Julander (2011) showed that the new extended-range temperature sensors recorded 1–2°C warmer than the standard sensors at the Trinity Mountain SNOTEL site located in Idaho, Inland Pacific Northwest. Generally such

inconsistency in temperature recording was observed at all of the Idaho SNOTEL sites (Julander, 2011). In a more recent study, Oyler et al. (2014) showed an artificial increase in warming trends at the Western US SNOTEL sites while evaluating temperature observations from 1991 to 2012. Systematic inconsistencies in the minimum temperature were noticed when high elevation SNOTEL temperatures were homogenized with the low elevation NCDC stations. They concluded an average of 1.42°C increase in minimum temperature as a result of replacement of temperature sensors from 1995 to 2006.

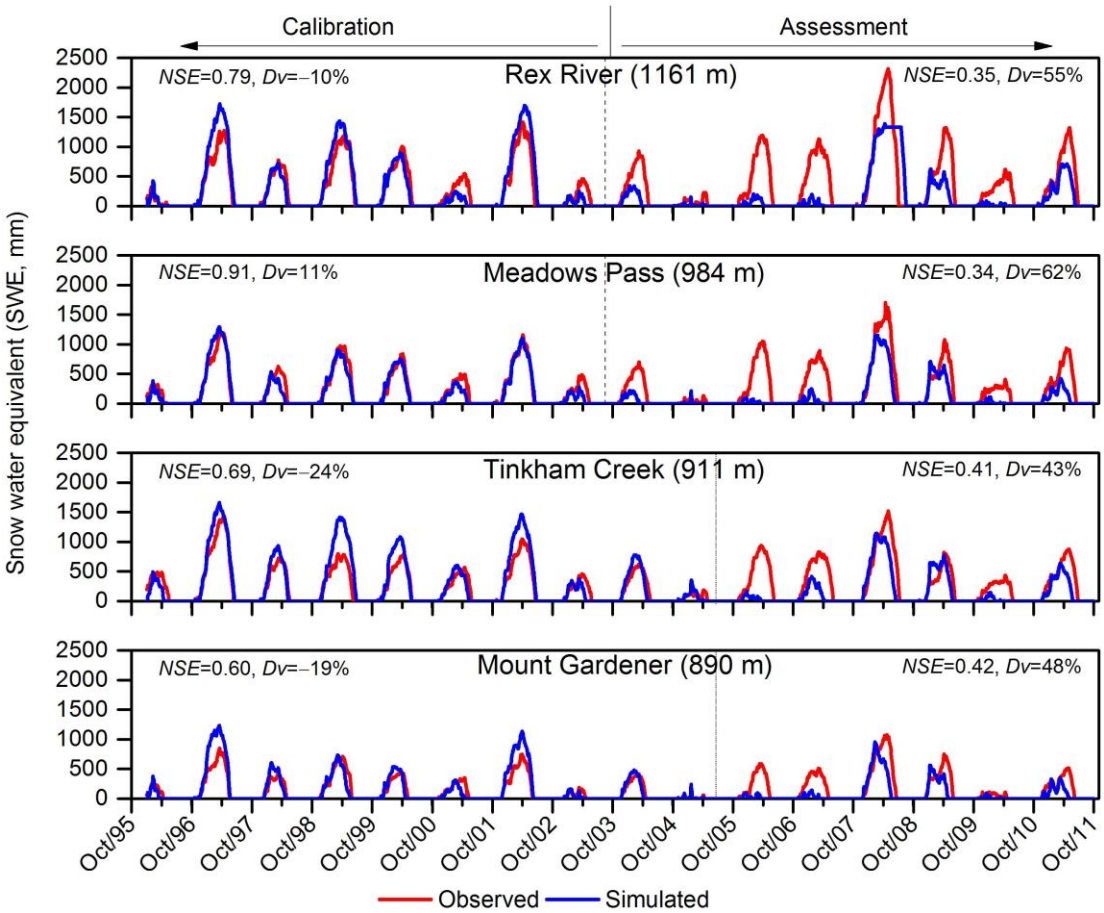

Fig. 3. Comparison of observed and WEPP-simulated daily SWE at four SNOTEL sites for the model calibration (1996–2003) and assessment (2004–2011) periods. Vertical lines indicate the period of the replacements of standard temperature sensors with the extended-range temperature sensors at the SNOTEL sites (Dashed line: July, 2003; Dotted line: May, 2005).

3.2 Streamflow

WEPP simulation results indicated that surface runoff was negligible, and that simulated streamflow consisted mainly of subsurface lateral flow and baseflow. Subsurface lateral flow accounted for 50% and 37%, and baseflow amounted to 50% and 63%, of the total streamflow, in winter and summer, respectively. The simulated streamflow peaks were composed largely of subsurface lateral flow, and low flows were contributed primarily by baseflow.

Surface runoff from undisturbed forests is rare due to the presence of groundcover and organic litter, which protects soil from raindrop impact, and enhances infiltration

(Elliot, 2013). In mountainous forests, water entering streams is typically subsurface lateral flow from the soil profile and baseflow from the underlying bedrock (Fiori et al., 2007; Bachmair and Weiler, 2011).

Comparison of WEPP-simulated and observed daily streamflow for the calibration period shows an underestimate of the peaks in winter and an overestimate of the peaks in spring, particularly for water years 1997 and 2002 (Fig. 4a). During the model assessment period, the streamflow peaks in both winter and spring were better simulated by WEPP, except for 2006 and 2007 (Fig. 4b).

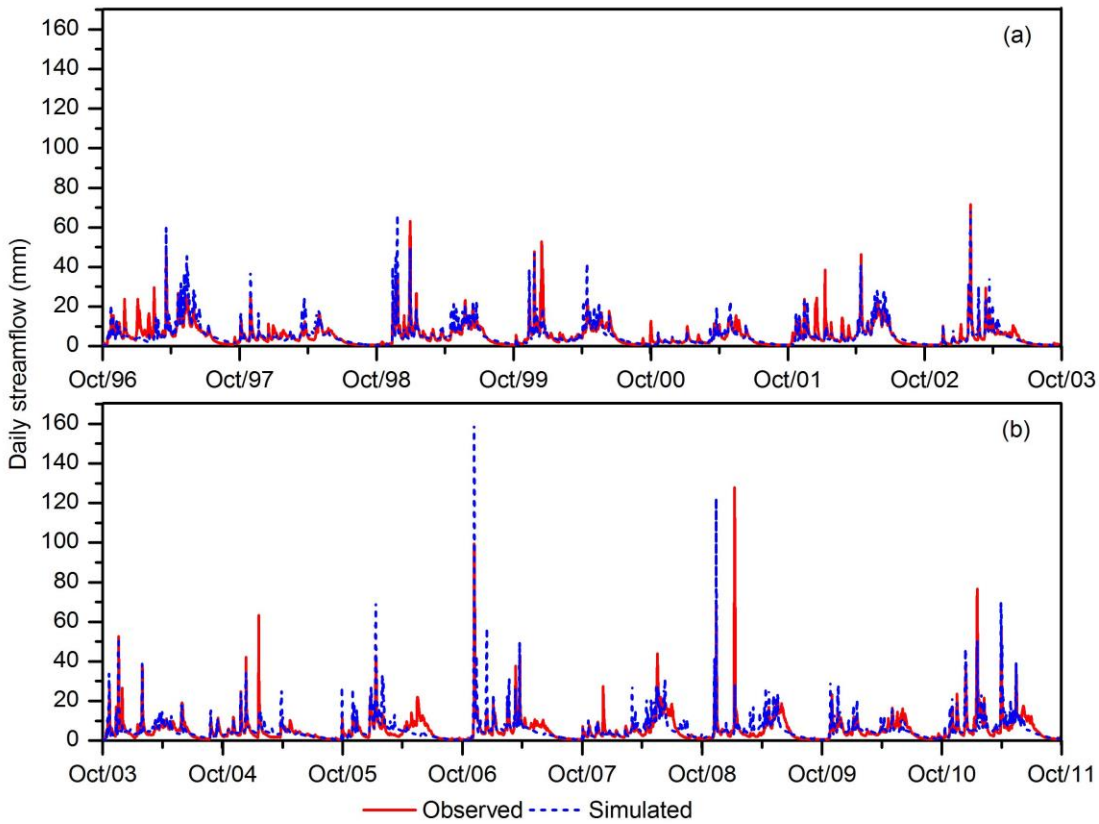

Fig. 4. Comparison of observed and simulated hydrograph for (a) model calibration (1996–2003), (b) assessment (2004–2011) periods.

The comparison of WEPP-simulated and observed winter processes for 1997 suggests that the actual temperature range for rain-snow partition may be lower than the calibrated, whereas such comparison for 2006 suggests the opposite, demonstrating the complexity and challenges in calibrating temperature thresholds for rain-snow partition and modeling snowmelt and accumulation impacted by microclimate and complex weather patterns.

3.3 Water Balance

Major water balance components for the whole watershed for the calibration and model assessment periods are presented in Table 4. The mean annual precipitation during 1996−2011 was 2552 mm. The simulated surface runoff from individual hillslopes was negligible at less than 0.002% of the total simulated streamflow. Simulated subsurface lateral flow ranged from 385 mm to 1447 mm, averaging 883

mm or 44% of annual streamflow over the entire 16-year period. The remainder of the streamflow was contributed by baseflow.

Annual *ET* from the watershed varied from 535 mm to 661 mm, averaging 601 mm or 23% of annual precipitation. Whitaker et al. (2003) and Link et al. (2004) reported simulated *ET* as 21% of annual precipitation for coniferous trees from watersheds located 415 km northeast and 405 km south of Cedar River watershed, respectively. In a study conducted on the east coast of Vancouver Island, British Columbia (225 km northwest of the Cedar River watershed), Jassal et al. (2009) measured *ET* for 58-, 19-, and 7-year-old coniferous forests using the eddy-covariance technique. Their measured yearly *ET* values were 27%, 25%, and 18% of annual precipitation, ranging from 1127 mm to 1913 mm in a 10-year period. The simulated *ET* in percent of the annual precipitation in our study is agreeable to the literature values.

Table 4. Simulated annual water balance for 1996–2011 water years.

Year		P (mm)	ET (mm)	D (mm)	SW (mm)	GW (mm)	$Q_{surf}+Q_{lat}$ (mm)	Q_b (mm)	Q_{seep} (mm)	BFI (%)
1996		1887	557	763	7	−61	563	820	4	59
1997		3462	644	1412	27	38	1447	1368	7	49
1998		2088	559	1078	−131	−38	620	1109	6	64
1999		3031	635	1310	−2	30	1198	1274	6	52
2000		2694	619	1136	97	−17	914	1148	6	56
2001		1754	650	841	−94	−8	385	846	4	69
2002		2825	611	1177	−9	24	1140	1147	6	50
2003		2063	535	846	73	−30	666	871	4	57
2004		2643	641	1234	45	111	795	1120	6	58
2005		2089	661	931	30	−105	520	1030	5	66
2006		2430	591	1066	−85	-8	902	1067	5	54
2007		2844	600	1136	−4	5	1145	1126	6	50
2008		2813	590	1239	12	44	1034	1190	6	54
2009		2577	588	1175	−47	−39	882	1208	6	58
2010		2442	574	1194	78	27	627	1163	6	65
2011		3194	564	1413	−63	−15	1298	1420	7	52
Calibration	Avg.	2475	601	1073	22	45	867	1073	5	55
(1996–2003)	% of *P*		24	43	0.90	1.83	35	43	0.22	
Assessment	Avg.	2629	601	1174	−47	−91	900	1165	6	56
(2004–2011)	% of P		22	45	1.58	3.50	35	45	0.22	
Overall	Avg.	2552	601	1122	−27	−47	883	1119	6	57
(1996–2011)	% of P		23	44	1.10	1.90	35	44	0.22	

P, precipitation, *ET*, evapotranspiration, *D*, deep percolation from soil profile, *SW* and *GW*, yearly change in soil- and groundwater, respectively calculated as the last day's value minus the first day's, Q_{surf}, surface runoff, Q_{lat}, subsurface lateral flow, Q_b , baseflow, Q_{seep}, deep seepage from groundwater reservoir, and *BFI*, baseflow index (baseflow in percent streamflow). The sum of Q_{surf}, Q_{lat}, and Q_b forms the total streamflow.

The WEPP-simulated annual baseflow varied from 820 mm to 1420 mm and formed the largest water balance component, accounting for 44% of the precipitation and 56% of streamflow yearly on average. This result is similar to that from a down-scaling analysis for our watershed of the comprehensive study by Santhi et al. (2008) using the USGS smoothed-minima method.

The *NSE* for streamflow for the calibration period ranged from 0.31 to 0.79 averaging 0.54, and D_v varied from −3 to 18% averaging 4%. The low value of *NSE* (0.31) in 1997 was reflective of WEPP's inadequacy in simulating winter streamflow peaks due to the overprediction of snow accumulation as previously discussed. For

the model assessment, *NSE* varied between −0.04 and 0.65 with an average of 0.43, and D_v from −3 to 7% with an average of 1%. The low *NSE* in 2005, 2006, and 2009 resulted from incorrect representation of the snow accumulation and melt processes. The positive values of D_v for both model calibration and assessment suggest that WEPP underpredicted the streamflow for the study watershed.

3.4 Groundwater Baseflow

The estimated initial groundwater storage was 85 mm, and varied daily from 13 mm to 340 mm, indicating yearlong groundwater flow to the stream. The simulated groundwater storage generally peaked during the snowmelt season of May–June, and declined to minimum by the end of the dry season in September–October.

The estimated k_b value of 1.99×10^{-2} d^{-1} suggests an average residence time for the baseflow was 50 days. The positive k_l value of 1.0×10^{-4} d^{-1} indicates a downward movement of water from the upper to the lower aquifer. The baseflow and deep seepage simulated using the linear-reservoir model followed the trend of groundwater storage with baseflow varying from 0.3 mm to 6.8 mm per day, and daily deep seepage from 0 to 0.03 mm, over the simulation period.

For the study area, no information about well sites and measurements of groundwater levels were available to independently verify the groundwater storage and baseflow coefficients. Safeeq et al. (2013) estimated a mean k_b value of 4.0×10^{-2} d^{-1} for groundwater-dominated, slow-draining watersheds receiving mixed rain and snow in the western US by relating the dynamics of snowpack and groundwater using daily streamflow data. In another study, Sanchez-Murillo et al. (2014) examined 26 watersheds that varied in size from 6 km^2 to 6,500 km^2 in the western US, and determined k_b as ranging from 0.02 d^{-1} for granitic watersheds to 0.08 d^{-1} for basalt and loess watersheds. For a small granitic watershed in the Priest River Experimental Forest in northern Idaho, Srivastava et al. (2013) estimated k_b and k_s to be 0.016 d^{-1} and 2.6×10^{-4} d^{-1}, respectively. The baseflow coefficients obtained in this study for the Cedar River watershed fall into the ranges reported in the literature.

4. SUMMARY AND CONCLUSIONS

Potential improvements to WEPP's groundwater hydrology and winter processes were evaluated on the mountainous Upper Cedar River watershed (105 km^2) in the US Pacific Northwest. The baseflow component, based on a linear-reservoir approach, was incorporated into the WEPP model for estimating groundwater contribution to streamflow. A double threshold temperature approach for rain-snow partition was implemented in WEPP to better simulate the snow accumulation and melt processes.

WEPP was calibrated using observed streamflow data for 1996–2003, and the model performance was evaluated for 2004–2011. The calibrated parameters included the threshold temperatures for rain-snow partition, Penman-Monteith mid-season crop coefficient, soil anisotropy ratio, and saturated hydraulic conductivity of the restrictive layer below the soil profile

Simulated annual water balance suggested that, on average, subsurface lateral flow and baseflow contribution to streamflow were 44% and 56%, respectively. The

estimated baseflow and deep seepage coefficients were 1.99×10^{-2} d^{-1} and 1.0×10^{-4} d^{-1}, respectively. An overall *NSE* of 0.48 and D_v of 3% demonstrate the applicability of the WEPP model to large watersheds dominated by groundwater baseflow.

The observed annual streamflow averaged 2062 mm for 1996–2011, while the simulated was 2003 mm. The small underprediction of streamflow may have been due to a slight overprediction of *ET*. Further research is needed to evaluate vegetation coefficients in the Penman-Monteith method and *ET* amounts for trees of different species and ages in forest watersheds receiving high precipitation.

The amount and timing of snow accumulation and melt are highly dependent on climatic conditions. Following replacement of the SNOTEL air temperature thermistors, simulated SWE was underpredicted by the model. Independent studies have confirmed that these new extended range thermistors may read 1-2°C warmer than the older sensors Were complete, field-measured climatic data available, it would likely help to improve hydrologic modeling.

REFERENCES

Abaci O, Papanicolaou ANT. 2009. Long-term effects of management practices on water-driven soil erosion in an intense agricultural sub-watershed: monitoring and modelling. *Hydrological Processes* 23: 2818–2837.

Allen RG, Pereira LS, Reas D, Smith M. 1998. Crop evapotranspiration: Guidelines for computing crop water requirement. Irri. And Drain. Pap. 56. Food and agriculture Organization of the United Nations, Rome. p300.

Amore E, Modica C, Nearing MA, Santoro VC. 2004. Scale effect in USLE and WEPP application for soil erosion computation from three Sicilian basins. *Journal of Hydrology* 293: 100–114.

Arnold JG, Williams JR, Srinivasan R, King KW. 1995. *SWAT: Soil Water Assessment Tool*. Texas A&M University, Texas Agricultural Experiment Station, Blackland Research Center, 808 East Blackland Road, Temple, TX.

Bachmair S, Weiler M. 2011. New Dimensions of Hillslope Hydrology. *In Forest Hydrology and Biogeochemistry.* SE-23 , Levia DF, Carlyle-Moses D, and Tanaka T (eds). Springer Netherlands. p455–481.

Baffaut C, Nearing MA, Ascough JC, Liu B. 1997. The WEPP watershed model: II. Sensitivity analysis and discretization on small watersheds. *Transactions of the ASAE* 40: 935–943.

Belcher WR, Sweetkind DS, Elliott PE. 2002. Probability Distributions of Hydraulic Conductivity for the Hydrogeologic Units of the Death Valley Regional Ground-water Flow System, Nevada and California: United States Geological Survey Water Resources Investigation Report 02-4212. p24.

Bourdin DR, Fleming SW, Stull RB. 2012. Streamflow Modelling: A Primer on Applications, Approaches and Challenges. *Atmosphere-Ocean* 50: 507–536.

Brooks ES, Elliot WJ, Boll J, Wu JQ. 2011. Assessing the Sources and Transport of Fine Sediment in Response to Management Practices in the Tahoe Basin using the WEPP Model. *http://www.fs.fed.us/psw/partnerships/tahoescience/documents/p005_BrooksFinalReportJan2011.pdf*.

Brutsaert W. 2008. Long-term groundwater storage trends estimated from streamflow

records: Climatic perspective. *Water Resources Research* 44: 1–7.
Chapman T. 1999. A comparison of algorithms for stream flow recession and baseflow separation. *Hydrological Processes* 13: 701–714.
Christensen L, Tague CL, Baron JS. 2008. Spatial patterns of simulated transpiration response to climate variability in a snow dominated mountain ecosystem. *Hydrological Processes* 22: 3576–3588.
Covert SA, Robichaud PR, Elliot WJ, Link TE. 2005. Evaluation of runoff prediction from WEPP-based erosion models for harvested and burned forest watersheds. *Transactions of the ASAE* 48: 1091–1100.
Dai A. 2008. Temperature and pressure dependence of the rain-snow phase transition over land and ocean. *Geophysical Research Letters* 35: L12802. DOI: 10.1029/2008GL033295
Dale VH, Hemstrom M, Franklin J. 1986. Modeling the long-term effects of disturbances on forest succession, Olympic Peninsula, Washington. *Canadian Journal of Forest Research* 16: 56–67.
Dooge JCI. 1960. The routing of groundwater recharge through typical elements of linear storage. Commission of Subterranean Waters. *International Association of Scientific Hydrology*. General Assembly of Helsinki Publication 52: 286–300.
Dun S, Wu JQ, Elliot WJ, Robichaud PR, Flanagan DC, Frankenberger JR, Brown RE, Xu AC. 2009. Adapting the Water Erosion Prediction Project (WEPP) model for forest applications. *Journal of Hydrology* 366: 46–54.
Dun S, Wu JQ, McCool DK, Frankenberger JR, Flanagan DC. 2010. Improving frost-simulation subroutines of the Water Erosion Prediction Project (WEPP) model. *Transactions of the ASABE* 53: 1399–1411.
Elliot, WJ. 2013. Erosion processes and prediction with WEPP technology in forests in the Northwestern U.S. *Transactions of the ASABE* 52: 563–579.
Elsner MM, Cuo L, Voisin N, Deems JS, Hamlet AF, Vano JA, Mickelson KEB, Lee S-Y, Lettenmaier DP. 2010. Implications of 21st century climate change for the hydrology of Washington State. *Climatic Change* 102: 225–260.
Federer CA. 2002. BROOK 90: A simulation model for evaporation, soil water, and streamflow. http://www.ecoshift.net/brook/brook90.htm.
Fenicia F, Savenije HHG, Matgen P, Pfister L. 2006. Is the groundwater reservoir linear? Learning from data in hydrological modelling. *Hydrology and Earth System Sciences* 10: 139–150.
Fiori A, Romanelli M, Cavalli DJ, Russo D. 2007. Numerical experiments of streamflow generation in steep catchments. *Journal of Hydrology* 339: 183–192.
Flanagan DC, Nearing MA. 1995. *USDA-Water Erosion Prediction Project: Hillslope profile and watershed model documentation*. NSERL Report No. 10. W. Lafayette, IN: USDA-ARS NSERL. p285.
Franklin JF, Dyrness CT. 1988. Natural vegetation of Oregon and Washington. Oregon State University Press, Corvallis, OR. p417.
Garbrecht J, Martz LW. 2000. Digital elevation model issues in water resources modeling. *Hydrologic and hydraulic modeling support with geographic information systems*. 1–28. http://proceedings.esri.com/library/userconf/proc99/proceed/papers/pap866/p866.htm.

Graham CB, van Verseveld W, Barnard HR, McDonnell JJ. 2010. Estimating the deep seepage component of the hillslope and catchment water balance within a measurement uncertainty framework. *Hydrological Processes* 24: 3631–3647.
Gupta HV, Sorooshian S, Yapo PO. 1999. Status of automatic calibration for hydrologic models: Comparison with multilevel expert calibration. *Journal of Hydrologic Engineering* 4: 135–143.
Hamlet AF. 2011. Assessing water resources adaptive capacity to climate change impacts in the Pacific Northwest Region of North America, Hydrol. Earth Syst. Sci. 15: 1427–1443, doi:10.5194/hess-15-1427-2011.
Henderson JA, Lesher RD, Peter DH, Shaw DC. 1992. Field guide to the forested plant associations of the Mt. Baker-Snoqualmie National Forest. Tech. Pap. R6. ECOL TP 028-91. US Department of Agriculture Forest Service, Pacific Northwest Research Station.
Hornberger GM, Raffensperger JP, Wiberg PL, Eshleman KN. 1998. *Elements of Physical Hydrology*. Johns Hopkins University Press: Baltimore.
Hubbart JA, Link TE, Elliot WJ. 2011. Strategies to improve WEPP snowmelt simulations in mountainous terrain. *Transactions of the ASABE* 54: 1333–1345.
Jassal RS, Black TA, Spittlehouse DL, Brümmer C, Nesic Z. 2009. Evapotranspiration and water use efficiency in different-aged Pacific Northwest Douglas-fir stands. *Agricultural and Forest Meteorology* 149: 1168–1178.
Julander RP. 2011. Uncertainty in Utah Hydrologic Data: Part 1 On The Snow Data Set. http://pielkeclimatesci.wordpress.com/2011/06/21/uncertainty-in-utah-hydrologic-data-by-randall-p-julander-guest-post/.
Kienzle SW. 2008. A new temperature based method to separate rain and snow. *Hydrological Processes* 22: 5067–5085.
Krakauer NY, Temimi M. 2011. Stream recession curves and storage variability in small watersheds. *Hydrology and Earth System Sciences* 15: 2377–2389.
Kuraś PK, Weiler M, Alila Y. 2008. The spatiotemporal variability of runoff generation and groundwater dynamics in a snow-dominated catchment. *Journal of hydrology* 352: 50–66.
Link TE, Flerchinger GN, Unsworth M, Marks D. 2004. Simulation of water and energy fluxes in an old-growth seasonal temperate rain forest using the simultaneous heat and water (SHAW) model. *Jour. of hydrometeorology* 5: 443–457.
Liu BY, Nearing MA, Baffaut C, Ascough JC. 1997. The WEPP watershed model: III. Comparisons to measured data from small watersheds. *Transactions of the ASAE* 40: 945–952.
Maillet E. 1905. *Essai d'hydraulique souterraine et fluviale.* Librairie scientifique A. Hermann: Paris.
Maurer EP, Mass C. 2006. Using radar data to partition precipitation into rain and snow in a hydrologic model. *Journal of Hydrologic Engineering* 11: 214–221.
Mizukami N, Koren V, Smith M, Kingsmill D, Zhang Z, Cosgrove B, Cui Z. 2013. The Impact of Precipitation Type Discrimination on Hydrologic Simulation: Rain–Snow Partitioning Derived from HMT-West Radar-Detected Brightband Height versus Surface Temperature Data. *Journal of Hydrometeorology* 14: 1139–1158.
Moore RD. 1997. Storage-outflow modelling of streamflow recessions, with

application to a shallow-soil forested catchment. *Jour. of Hydrology* 198: 260–270.
Nash JE, Sutcliffe JV. 1970. River flow forecasting through conceptual models part I—A discussion of principles. *Journal of hydrology* 10: 282–290.
Nathan RJ, McMahon TA. 1990. Evaluation of automated techniques for base flow and recession analyses. *Water Resources Research* 26: 1465–1473.
Nearing MA, Foster GR, Lane LJ, Finkner SC. 1989. A process-based soil erosion model for USDA-Water Erosion Prediction Project technology. *Transactions of the ASAE* 32: 1587–1593.
Nicks AD, Lane LJ, Gander GA. 1995. Weather generator. In: *Flanagan DC, Nearing MA, eds. USDA-Water Erosion Prediction Project: Hillslope profile and watershed model documentation*. NSERL Report No. 10. W. Lafayette, IN: USDA-ARS NSERL.
Oyler JW, Dobrowski SZ, Ballantyne AP, Klene AE, Running SW. 2015. Artificial amplification of warming trends across the mountains of the western United States. *Geophysical Research Letters* 42: 153–161, doi:10.1002/2014GL062803.
Pandey A, Chowdary VM, Mal BC, Billib M. 2008. Runoff and sediment yield modeling from a small agricultural watershed in India using the WEPP model. *Journal of Hydrology* 348: 305–319.
Renschler CS. 2003. Designing geo-spatial interfaces to scale process models: The GeoWEPP approach. *Hydrological Processes* 17: 1005–1017.
Safeeq M, Grant GE, Lewis SL, Tague CL. 2013. Coupling snowpack and groundwater dynamics to interpret historical streamflow trends in the western United States. *Hydrological Processes* 27: 655–668.
Sánchez-Murillo R, Brooks ES, Elliot WJ, Gazel E, Boll J. 2014. Baseflow recession analysis in the inland Pacific Northwest of the United States. *Hydrogeology Journal* 23: 287–303.
Santhi C, Allen PM, Muttiah RS, Arnold JG, Tuppad P. 2008. Regional estimation of base flow for the conterminous United States by hydrologic landscape regions. *Journal of Hydrology* 351: 139–153.
Savabi MR, Young B, Benoit GR, Witte J, Flanagan D. 1995. Winter hydrology. In USDA *Water Erosion Prediction Project: Technical Documentation*, Chapter 3: 14. NSERL Report No. 10. D.C. Flanagan and M.A. Nearing, eds. West Lafayette, IN: National Soil Erosion Research Laboratory.
Seattle Public Utilities. 2014. [Accessed on 3/5/2014]. http://www.seattle.gov.
Shellberg JG, Bolton SM, Montgomery DR. 2010. Hydrogeomorphic effects on bedload scour in bull char (Salvelinus confluentus) spawning habitat, western Washington, USA. *Canadian Jour. of Fisheries and Aquatic Sciences* 67: 626–640.
Singh VP. 1997. Effect of spatial and temporal variability in rainfall and watershed characteristics on streamflow hydrograph. *Hydrologic Processes*. 11: 1649–1669.
Smith CD. 2007. The relationship between monthly precipitation and elevation in the Alberta foothills during the Foothills Orographic Precipitation Experiment, Cold Region Atmospheric and Hydrologic Studies (The Mackenzie GEWEX Experience) Volume I: Atmospheric Dynamics, Ming-ko Woo (ed), Springer, NY.
Srivastava A, Dobre M, Wu JQ, Elliot WJ, Bruner EA, Dun S, Brooks ES, Miller IS. 2013. Modifying WEPP to improve streamflow simulation in a Pacific Northwest watershed. *Transactions of the ASAE* 56: 603–611.

Storm B, Punthakey JF. 1995. Modelling Environmental changes in the Wakool Irrigation District. MODSIM 95, *International Congress on Modelling and Simulation Proceedings, Newcastle, Australia* 3: 47–52.

Tague C, Grant GE. 2009. Groundwater dynamics mediate low-flow response to global warming in snow-dominated alpine regions. *Water Resources Research* 45, *W07421,* doi:10.1029/2008WR007179.

Todd DK, Mays LW. 2005. *Groundwater Hydrology*. John Wiley & Sons: New York.

United States Army Corps of Engineers. 1956. *Snow Hydrology: Summary Report of the Snow Investigations*. North Pacific Division, Corps of Engineers, US Army.

USDA (United States Department of Agriculture). 2012. The US General Soil Map (STATSGO2) [King County, WA]. Available online at http://websoilsurvey.nrcs.usda.gov/. Accessed [09/6/2013].

USGS National Atlas of the United States. [Accessed on 3/5/2013]. http://nationalatlas.gov.

van Dijk AIJM. 2010. Climate and terrain factors explaining streamflow response and recession in Australian catchments. *Hydrology and Earth System Sci.* 14: 159–169.

Vetterling WT, Teukolsky SA, Press WH, Flannery BP. 1992. *Numerical Recipes*. Cambridge University Press: New York.

Vogel RM, Kroll CN. 1992. Regional geohydrologic-geomorphic relationships for the estimation of low-flow statistics. *Water Resources Research* 28: 2451–2458.

Wang L, Wu JQ, Elliot WJ, Dun S, Lapin S, Fiedler FR, Flanagan DC. 2010. Implementation of channel-routing routines in the Water Erosion Prediction Project (WEPP) model. *Proceedings of the 4th SIAM Conference on Mathematics for Industry (MI09)*. p120–128.

Whitaker A, Alila Y, Beckers J, Toews D. 2003. Application of the distributed hydrology soil vegetation model to Redfish Creek, British Columbia: Model evaluation using internal catchment data. *Hydrological processes* 17: 199–224.

Wiley MW, Palmer RN. 2008. Estimating the impacts and uncertainty of climate change on a municipal water supply system. *Journal of Water Resources Planning and Management* 134: 239–246.

Winter TC, Harvey JW, Franke OL, Alley WM. 1998. Ground water and surface water: a single resource. *United States Geological Survey Circular 1139*.

Wittenberg H. 1999. Baseflow recession and recharge as nonlinear storage processes. *Hydrological Processes* 13: 715–726.

Wittenberg H. 2003. Effects of season and man-made changes on baseflow and flow recession: case studies. *Hydrological Processes* 17: 2113–2123.

Wittenberg H, Sivapalan M. 1999. Watershed groundwater balance estimation using streamflow recession analysis and baseflow separation. *Jour. of Hydrology* 219: 20–33.

Wu H, Kimball JS, Elsner MM, Mantua N, Adler RF, Stanford J. 2012. Projected climate change impacts on the hydrology and temperature of Pacific Northwest rivers. *Water Resources Research* 48, W11530, doi:10.1029/2012WR012082.

Zecharias YB, Brutsaert W. 1988. Recession characteristics of groundwater outflow and base flow from mountainous watersheds. *Water Resources Research* 24: 1651–1658.

Zhang JX, Wu JQ, Chang K, Elliot WJ, Dun S. 2009. Effects of DEM source and resolution on WEPP hydrologic and erosion simulation: a case study of two forest watersheds in northern Idaho. *Transactions of the ASAE* 52: 447–457.